J Nanopart Res (2022) 24: 18
https://doi.org/10.1007/s11051-022-05407-5

RESEARCH PAPER

Hydrated zirconia nanoparticles as media for electrical charge accumulation

Artem Shylo · Igor Danilenko · Oksana Gorban · Oleksandr Doroshkevich · Igor Nosolev · Tetyana Konstantinova · Andriy Lyubchyk

Received: 23 September 2021 / Accepted: 11 January 2022 / Published online: 15 January 2022

Abstract This study is devoted to creating media for the accumulation of electrical energy based on zirconia nanoparticles. The effect of charge accumulation by compacted zirconia nanoparticles, the manifestation of which depends on the size of the particles and the degree of hydration of their surface, was found. It is shown that for the system of hydrated nanoparticles, the formation of the dielectric constant of the entire structure as a whole is influenced by the dielectric properties of the nanoparticle materials and water on its surface. The difference in the dielectric properties of the filler (water) and the matrix (material of zirconia nanoparticles) leads to a strong increase in the dielectric constant of hydrated compacted nanoparticles due to the Maxwell–Wagner effect, which is a promising application in the development of energy storage media.

A. Shylo (✉) · I. Danilenko · O. Gorban · O. Doroshkevich · I. Nosolev · T. Konstantinova
Materials Science Department, Donetsk Institute for Physics and Engineering named after O.O. Galkin of NAS of Ukraine, Kyiv, Ukraine
e-mail: art.shylo@gmail.com

O. Doroshkevich
Frank Laboratory of Neutron Physics, Joint Institute for Nuclear Research, Dubna, Russia

A. Lyubchyk
NANOTECHCENTER, Kyiv, Ukraine

A. Lyubchyk
Lusófona University, Lisbon, Portugal

Keywords Zirconia nanoparticles · Hydration · Charge accumulation · Dielectric properties · Environmental effects

Introduction

Energy consumption is continuously increasing and presently energy supply is an important problem. Electricity demand is expected to escalate by more than two times in 2050 and more than three times by the end of the twenty-first century (Lewis et al. 2005; Nguyen and Montemor 2019). Fossil fuels are the main source of electrical energy, but the decrease in the world stock of raw materials and increase in carbon dioxide emissions into the atmosphere during the production of electric power cause environmental problems. As a consequence, a tendency to develop and increase the amount of renewable energy became relevant. For example, one of the ways for energy harvesting from alternative sources of renewable energy (waste heat) is using thermoelectric generators that enable the conversion of waste heat into electricity. The use of waste heat as the energy source for thermoelectric generators is an economical option as it is both free and readily available [Singh, Y., Singh, S.K. & Hazra, P. The Quest for High-Efficiency Thermoelectric Generators for Extracting Electricity from Waste Heat. JOM (2021). https://doi.org/10.1007/s11837-021-04976-5].

The production of electricity from renewable sources is in most cases decentralized and intermittent. This entails a mismatch between energy consumption and supply, and it results in energy losses and low efficiency. Thus, the development of an intelligent, digital, and flexible system for the supply of electrical energy with a significant share of distributed energy sources is an actual task. This dictates the corresponding requirements for the creation of new materials and technologies for the accumulation and transformation of electrical energy. The current level of development of nanotechnology can improves storage capacitance, response speed, and service life of electrical energy storage devices.

A promising direction in this direction is the use of oxide nanomaterials as a functional media. So, oxide structures based on copper oxide (CuO) with particle size is about 20 nm, when used as an electrolyte H_2SO_4, which showed high values of specific density of about 158 F g^{-1} in 5 mVs^{-1} (Pendashteh et al. 2014). On mesoporous binary nickel–cobalt oxyhydroxides (Ni-Co), the specific capacitance density of 636 F g^{-1} with a cell voltage 2 V was obtained (Hsu et al. 2013). However, these systems use acids as the electrolytes, which are hazardous to use and not environmentally friendly. Replacing such materials or processes of their production with less harmful materials for humans and the environment, cheap and easy to use, is an actual task.

Interesting in this use are materials based on zirconia. Due to the unique combination of physical, mechanical, chemical, and electrophysical properties, zirconia is multifunctional material for a wide range of applications, in particular in energy, medicine, chemistry, mechanical engineering, and catalysis both in powder and monolithic state (Thakare 2012; Kelly and Denry 2008; Yin et al. 2017; Danilenko et al. 2017). The relatively high dielectric constant ($\varepsilon = 23$) (Thompson et al. 1992), the relatively wide surface spectrum of states (Lewis and Bronsted centers), which are easily changed due to external influences and high diffuse activity of ions of the surface layer (Maier 2005) of zirconia nanoparticles (NPs) make this material attractive for development of media for the accumulation of electrical energy. A large specific surface area of zirconia NPs causes an increased level of surface energy of NPs, which, in turn, leads to an increase in the activity of NPs, namely, increases the interaction between them and the environment in which they are located (Andrievsky and Ragulya 2005). It should be noted, the tendency to water absorption by NPs of zirconia (Lyubchyk et al. 2017), which gives a reason to consider them as a dispersed system; the particles of which are covered with an adsorbed layer of water. In such systems, electrokinetic phenomena mainly occur in the surface layers — within the dispersed phase and adsorbed (liquid) material. That is, NPs of a wide-gap dielectric based on ZrO_2 can be used as a media for electric energy storage devices. It should be noted, the nontoxic nature and wide availability of materials based on zirconia.

The choice of the tetragonal modification of zirconia is caused by the high adsorption of water molecules in comparison with monoclinic and cubic modifications and the possibility of changing the type of surface centers on the surface of nanoparticles depending on the temperature of their synthesis.

This work is aimed at studying the dielectric properties of hydrated compacted zirconia NPs under the influence of an external constant electric field. For the system of an ensemble of compacted NPs/layer of water adsorbed on its surface, one should expect that the formation of the dielectric constant of the entire structure as a whole should be influenced by both the dielectric properties of the nanoparticle material and the dielectric properties of water on the surface of NPs and in pores, which is a promising application in the development of media for the storage of electrical energy.

Material and methods

As an object of investigation, a nanopowder of composition $ZrO_2 + 3$ mol% Y_2O_3 with different annealing temperature compacted in the form of tablets was used. Production of nanopowders of composition ZrO2 − 3 mol% Y2O3 was carried out by the co-precipitation method of hydroxides from hydrochloric and nitric acid solutions of salts, taken in a stoichiometric ratio, with an aqueous solution of ammonia at a hydrogen value of $pH > 9$ (Konstantinova et al. 2011). All chemicals were of chemical purity. At first, an appropriate amount of Y_2O_3 was dissolved in nitric acid; then, the zirconium and yttrium salts were mixed in a propeller stirrer for 30 min and then added to an aqueous precipitant

solution (25% NH_4OH) with constant stirring. The precipitate was stirred for 1 h at room temperature at pH 9 for complete precipitation. Then, the precipitates were washed several times and filtered with distilled water. During the reaction, an insoluble precipitate — a hydrogel of amorphous zirconium hydroxide with dopant of $Y(OH)_3$ was formed. Drying of the hydrogel of amorphous zirconium hydroxide was performed in a microwave oven. To obtain crystalline particles, amorphous zirconium hydroxide was subjected to heat treatment in the isothermal mode at temperatures of 400, 500, 600, 700, 800, 900, and 1000 °C, 2 h. Heat treatment was carried out in electric resistance furnace. Y_2O_3 was added as stabilizing impurity in the crystal lattice of zirconia to eliminate volumetric changes in the crystalline lattice, which occur during phase transformation. Cations of Y_2O_3 form a solid substitution solution in the zirconium lattice. The addition of 3% mol Y_2O_3 stabilizes the tetragonal phase of polymorphic modification of zirconia. A further increase in the amount of yttrium oxide leads to the existence of a two-phase region of the tetragonal and cubic phases.

From the obtaining nanopowders using preliminary uniaxial pressure (P_{comp} = 40 MPa) cylindrical shape samples were formed (diameter 20 mm, thickness 2 mm, m = 1 g), and after that, the samples (compact sets) were pressed isostatically (CIP) at 500 MPa.

To determine the structural parameters and phase composition of objects under investigation, X-ray diffraction analysis by means a Dron-3 diffractometer with Cu-Kα radiation was used. The phase compositions of the nanopowders were determined using the equations (Chysovitina et al. 1991). The size of the coherent scattering area (CSA) in the studied nanopowders was estimated using Debay-Scherer equation (Patterson 1939):

$$D_{hkl} = \frac{m \cdot \lambda}{\beta \cdot \cos\theta} \quad (1)$$

where m = 0,9; λ is the wavelength of radiation; β is the physical extension of the interference maximum *hk*l; and cos θ is the value for reflection *hk*. The degree of crystallinity of tetragonal nanopowders was evaluated from the ratio of the area under the peak (111) under study with the reference sample (tetragonal zirconia, T = 1500 °C). The deviation in determination of phase composition was 5% and for determination of coherent scattering area was 10%.

The specific surface area (S_{BET}) of nanopowders and compact sets were determined by the BET method (Brunauer, Emmett, Teller) using device SORBI-4. Before measurement, the nanopowders and compact sets were heat treated at 140 °C for 30 min to remove adsorbed water. The obtained data were processed using SoftSorbi – II ver.1.0 software. The deviation of determination of specific surface area was less than 1%.

The powders were also studied by transmission electron microscopy (TEM) (Jem 200A, JEOL, Japan) and scanning electron microscopy (SEM) (JSM 6490LV, Jeol, Japan).

To determine the values of density and open porosity of nanopowders after exposure to CIP, the hydrostatic weighing method was used.

Saturation of the compact sets by water within a certain time (1 h) was measured gravimetrically. Amount of water in the samples was calculated by the formula:

$$\Delta m = \frac{m - m_0}{m_0}, \quad (2)$$

where m_0 and m are the masses of the dehydrated and hydrated compact set, respectively.

To study the effect of a constant electric field on the electrical properties of the compact sets, an experimental unit, which assumes two-position switching of the sample electrodes on the power supply and on the ohmic load (R_{load} = 1 MOhm), was used. During measurement of charge–discharge characteristics, the compact sets were placed in a climate chamber (relative humidity varied from 20 to 85%). The magnitude of the applied external electric field was 5 V/mm. Measurements were performed using a multimeter AM1199 with a deviation of 1%.

Electrochemical impedance spectroscopy (EIS) measurements were carried out using precision virtual meter-analyzer of impedance parameters 2 V – 1 in the frequency range from 1 Hz to 1 MHz. In order to ensure the linearity of the studied electrochemical system, the amplitude of the applied alternating excitation signal was limited to 50 mV. Before EIS measurements, the compact sets were saturated with moisture at 80% relative humidity in the climate chamber

until the change in the absorption of moisture by the samples stopped.

The frequency dependences of the voltage on the sample and the reference resistor were recorded, from which the values of resistance R, capacitance C, and tangent of the dielectric loss tgδ were calculated, from which the values of the imaginary Z′ and the real Z″ components of the total complex resistance Z were calculated. The values of the real (ε′) and imaginary (ε″) parts of the relative permittivity were calculated from the values of Z′ and Z″. The Debye model with Cole–Davidson relaxation time distributions was used for approximation of the experimental data.

Carbon electrodes were deposited on the wide faces of the samples.

It should be noted that all measurements were repeated 3 times and the estimated standard deviation did not exceed 3%.

Nanoparticles and compact sets characterization

The effect of annealing temperature on the phase composition of nanopowders is shown in Fig. 1. As the annealing temperature increases, the phase composition of the powders practically do not change — the crystalline phase of zirconia with a tetragonal lattice of the P42/nmc type remains which correspond to lattice planes hkl that are shown in Table 1. The observed X-ray reflections exhibit good agreement with the ICDD standard card No. 01–078-1765. In Table 2, the phase composition, degree of crystallinity, and CSA for nanopowders obtained at different synthesis temperatures are shown. As can be seen, particle size of NPs depends on the synthesis temperature and increases from 9 to 32 nm with an increase in the synthesis temperature from 400 to 1000 °C. All nanopowders under investigation have close degree of crystallinity (˃ 85%). The formation of 2–3% of the monoclinic phase (P21/s) at high calcination temperatures is associated with the influence of the dimensional effect on the phase transformation (Kelly and Denry 2008; Chevalier and Gremillardw 2009).

Transmission electron microscopy data for nanopowders synthesized at temperatures of 400, 700, and 1000 °C are shown in Fig. 2a. As can be seen from the data presented, the particle size increases with an increase in the powder annealing temperature, and the degree of powder aggregation also changes. As shown in Konstantinova et al. (2011); Doroshkevich et al. 2010), the agglomeration of small particles of zirconia nanopowders synthesized at low temperatures (400 °C) is caused by van der Waals forces, and at high (900–1000 °C) — by the beginning of sintering of NPs. A good correlation between the particle sizes measured from X-ray structural analysis

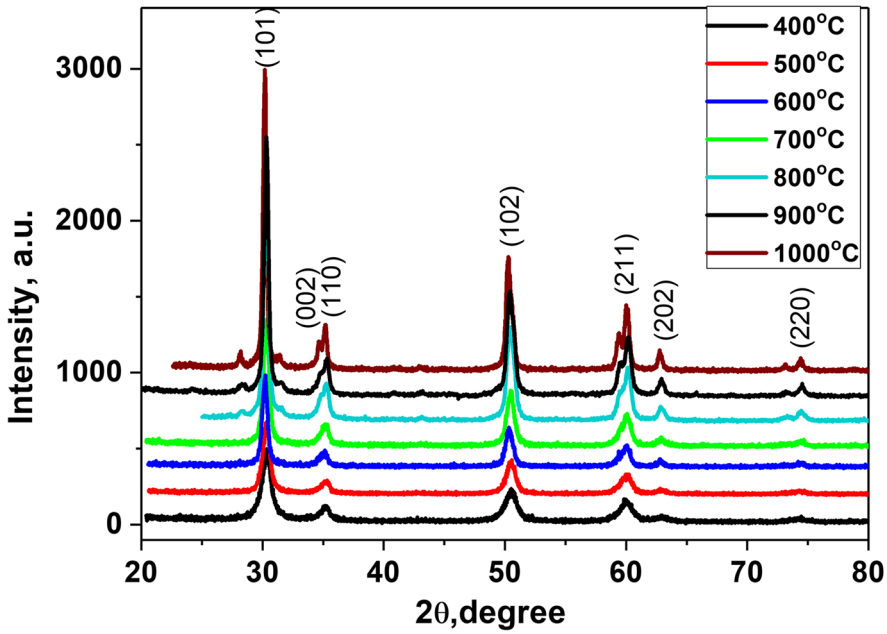

Fig. 1 The effect of annealing temperature on the phase composition of zirconia NPs

Table 1 XRD data (hkl indices and corresponding parameters) for tetragonal zirconia

h	k	l	2θ, deg	D, E	I, rel	F(hkl)	FWHM
1	0	1	30.212	2.95580	100	65.56	0.822
0	0	2	34.696	2.58338	8.38	44.1	0.846
1	1	0	35.190	2.54824	13.58	40.3	0.849
1	0	2	43.046	2.09963	1.27	10.91	0.894
1	1	2	50.251	1.81418	38	71.01	0.939
2	0	0	50.618	1.80188	20.08	73.6	0.941
2	0	1	53.84	1.70139	0	0	0.962
1	0	3	59.434	1.55392	14.22	52.55	1
2	1	1	60.089	1.53854	27.47	52.29	1.005
2	0	2	62.827	1.4779	6.99	39.19	1.025
2	1	2	68.574	1.36738	0.4	7.26	1.069
0	0	4	73.218	1.29169	2.33	53.03	1.107
2	2	0	74.396	1.27412	5.77	59.9	1.117
2	0	3	76.443	1.24502	0	0	1.135
1	0	4	78.618	1.21594	0.33	10.67	1.155

Table 2 Phase composition and sizes of zirconia NPs

Parameters	T, °C						
	400	500	600	700	800	900	1000
Crystalline phase, %	100%T	100%T	100%T	100%T	100%T	100%T + marks M	98%T + 2%M
CSA, nm	9	11	15	19	22	26	32
Degree of crystallinty, %	86	88	93	96	100	100	100

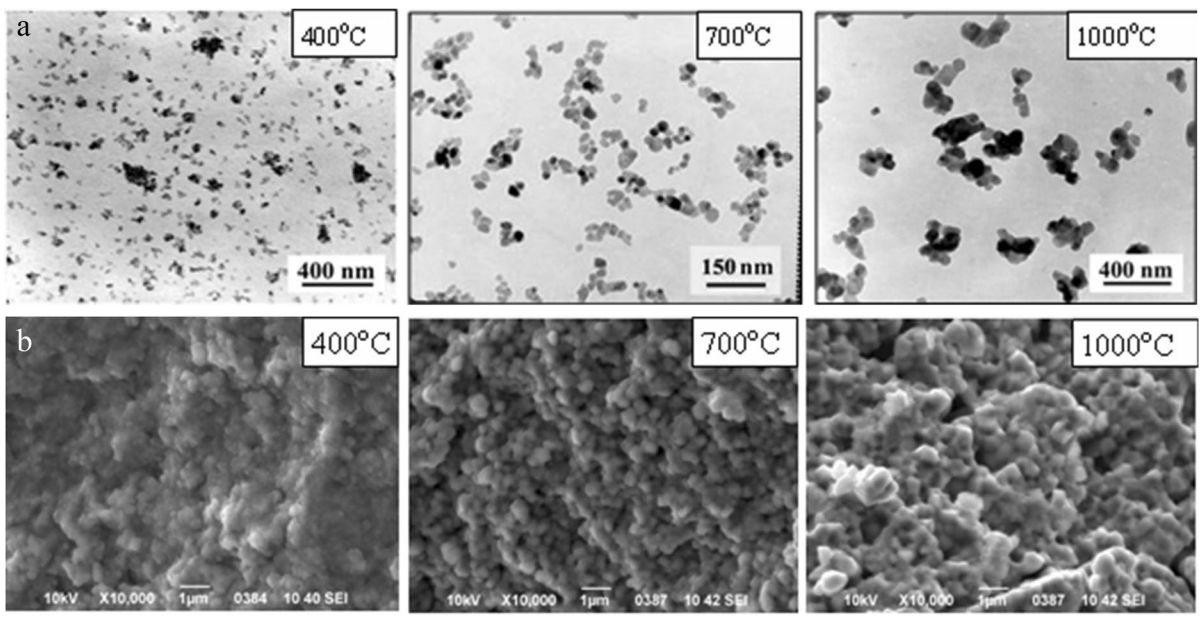

Fig. 2 TEM images of NPs (**a**) and surface morphology of compacted NPs (**b**) synthesized at different annealing temperatures (T = 400, 700, 1000 °C)

and TEM data indicates that NPs are single-crystal objects.

Photomicrographs of the fracture surface of compacts obtained from nanopowders with different annealing temperatures are shown in Fig. 2b. The value of the applied pressure is 500 MPa. It is seen that all compacts have a homogeneous microstructure.

Characteristics of NPs and compact sets, measured by the BET method, are shown in Table 3. As can be seen, specific surface areas of the NPs $S_{BET\ NP}$ decrease with an increase in their annealing temperature. The porosity of the NPs also decreases with an increase in the annealing temperature, which indicates the processes of particles combining, first by the method of oriented attachment (Konstantinova et al. 2006), and later — the beginning of the process of sintering NPs and the formation of tight aggregates.

The values of *C* (constant BET) for NPs with synthesis temperature T = 500–1000 °C are approximately the same regardless of their annealing temperature, which indicates the same nature of the energy interaction of the adsorbent/adsorbate. At the same time, the constant *C* for a NPs with T = 400 °C is much less, which indicates a different nature of the interaction between the particle surface and the adsorbate. This indicates a change in the adsorption capacity of nanopowders, which is confirmed by the data of measuring the amount of adsorbed water Δm in compacted nanopowders, which were placed at a relative atmospheric humidity of 80%, calculated according to (2). It can be seen that the amount of water adsorbed in the samples decreases with an increase in the synthesis temperature of nanopowders. Thus, the amount of adsorbed moisture in 5.8 times higher for compact sets obtained from NPs with annealing temperature T = 400 °C compared to samples obtained from NPs with annealing temperature T = 1000 °C.

Dependences of the values of density and open porosity of compacted NPs with different annealing temperatures obtained by the hydrostatic weighing method are shown in Table 4. As can be seen, the value of the density increases, and the porosity decreases with an increase in the annealing temperature of the NPs. With a decrease in the particle size, the density of the porous compacted samples is lower than in the case of microsized powders. This, in opinion of the authors (Groza and Dowding 1996), is caused by an increase in the forces of interparticle friction and an increase in the adsorption of gases, including water, on the surface of NPs.

Thus, a model object for research can be represented as a uniform and isotropic packing of dielectric NPs covered with an adsorbed layer of water. In this case, the size of NPs increases, and the amount of water adsorbed on their surface decreases with an increase in the synthesis temperature. Taking into account the effect of the particle size, the degree of aggregation, and porosity on the density of NPs after treatment under CIP conditions, it can be established

Table 3 Estimated characteristics of nanopowders and compact sets with different annealing temperatures according to the BET method and gravimetric analysis

Parameters	T, °C						
	400	500	600	700	800	900	1000
$S_{BET\ NP}$, $m^2\ g^{-1}$	170.0 ± 1.3	110.4 ± 1.8	80.5 ± 0.8	50.3 ± 0.6	41.6 ± 0.6	31 ± 0.4	21.5 ± 0.3
C	49	87	79	78	82	81	78
$V_{r < 19\ nm}$, $cm^3\ g^{-1}$	0.194	0.163	0.118	0.081	0.067	0.04	0.031
$S_{BET\ Cs}$, $m^2\ g^{-1}$	45.1 ± 0.7	80.3 ± 0.7	56 ± 0.5	39 ± 0.5	28 ± 0.4	22 ± 0.3	15 ± 0.3
Δm, %	6.5	5.22	4.24	2.52	2.12	1.55	1.12

Table 4 Dependence of the density and porosity of compacted NPs on the temperature of their synthesis

Parameters	T, °C						
	400	500	600	700	800	900	1000
Density, $g\ cm^{-3}$	2.75	2.83	2.91	3.01	3.03	3.06	2.96
Porosity, %	54	53	52	50	49	49	51

that an increase in interparticle contacts makes it possible to consider compacted powder systems as an intermediate object between a highly dispersed powder system and a bulk ceramic object and, therefore, can be affected by methods for studying electrical properties used to describe ceramic objects.

Results and discussion

In this section, we study the electrical properties of compacted zirconia NPs under the action of an external electric field in order to clarify the possibility of their use as media for energy storage.

Time dependences of the potential at the electrodes of compact sets from zirconia NPs obtained at different annealing temperatures after switching off the electric field are shown in Fig. 3. As seen from Fig. 3, a potential difference arises at the electrodes of the compact sets, which decreases exponentially with the discharge time. The dependences of the electric potential for NPs annealed at different temperatures have a similar shape. With an increase in the NPs annealing temperature from 400 to 1000 °C, the level of voltage decreases from 1.73 V to 0.22 V (Fig. 3), which leads to a more rapid loss of the polarized state by the compact sets. In particular, for compact sets consisting of powder with T = 400 °C, the level of potential difference in 2 times is greater, and the discharge time (the time during which the value of the potential difference drops by a factor of e ($e = 2.72$), the base of the natural logarithm) in 2.5 times is longer than for the samples consisting of NPs with T = 700 °C. A further increase in the annealing temperature leads to a significant decrease in the potential difference. At T = 1000 °C, the detected effect is close to zero (the initial level of potential difference is 22 mV). The discharge time is also significantly reduced: for samples consisting of particles with T = 400 °C, it is in 9 times longer than the particles with T = 1000 °C.

Time dependences of the potential difference at the electrodes of the compact sets in Fig. 3 have an exponential character and are described by the expression (Lewandowski et al. 2013):

$$U = U_0 \exp(-\frac{\Delta t}{R_0 C}), \quad (3)$$

where U_0 is the value of the potential difference at the moment the field is turned off; Δt is the discharge time, R_0 is the external load, and C is the capacitance of the system.

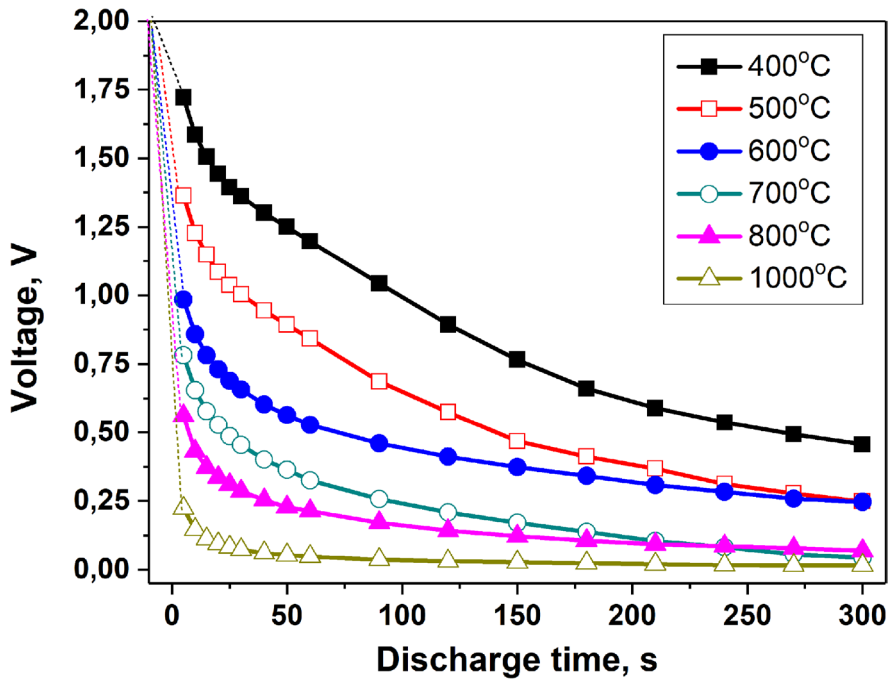

Fig. 3 Time dependences of the potential on the electrodes of compact sets after switching off the electric field for compact sets consisting of NPs obtained at different annealing temperatures

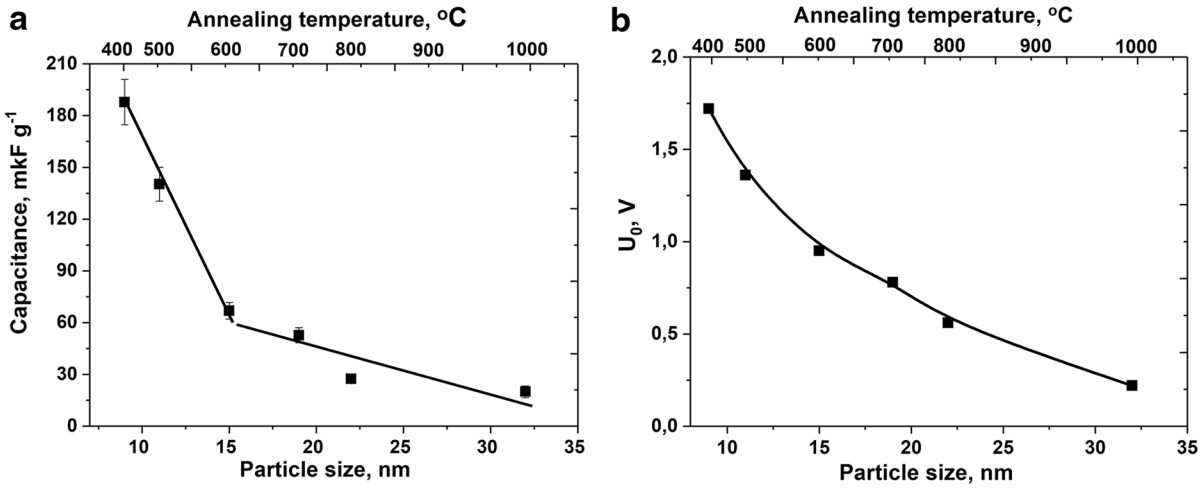

Fig. 4 Dependence on the size of particles (annealing temperature), compacted at 500 MPa: **a** the capacitance; **b** the potential difference U_0 at the electrodes at the initial moment of the discharge

The specific capacitance of the compact sets was determined based on (2):

$$C_S = \frac{\Delta t}{m \cdot R_0 \ln \frac{U_0}{U}}, \tag{4}$$

where m is the mass of the compact set.

The current value of the voltage U was determined from the ratio $U_0/U = e$.

Dependences of the specific capacitance of compact set C_S and the level of potential difference U_0 at the electrodes of compact sets at the initial instant of the discharge on the size (annealing temperature) of NPs are shown in Fig. 4a and b, respectively. As can be seen, the value of both the specific capacitance of the compact sets and the potential difference on the electrodes exponentially decreases with an increase in the size of the particles. The maximum value of the capacitance $C_{max} = 187$ μF g^{-1} and the potential difference at the electrodes $U_{0max} = 1.72$ V are achieved for compact sets, the particle size in which d = 9 nm. For samples consisting of the largest particles (d = 32 nm), the capacitance in almost 10 times less and is $C_{min} = 19.2$ μF g^{-1}, and the potential difference in 8 times less is $U_{0min} = 0.22$ V.

Since in the sample, apart from the nanoparticles themselves and the water adsorbed on its surface, there are no more elements, for example, an ion-exchange insulating membrane to prevent the penetration of ions between the electrodes and to protect supercapacitor from internal short, it is more correct to consider compacted zirconia nanoparticles as a capacitor. In the simplest case, compacted zirconia nanoparticles can be viewed as a flat capacitor — carbon contacts are separated by a dielectric layer (hydrated zirconia nanoparticles).

Based on the typical dependence of the capacitance of a plate capacitor on the specific surface of the material:

$$C = \frac{\varepsilon \varepsilon_0 S_{BET}}{d}, \tag{5}$$

where ε is the electric constant of material, ε_0 is the electric constant, and d is the distance between plates, we should obtain a linear dependence of the capacitance on the specific surface area. The processing of the experimental data on Fig. 5 showed that the linear dependences $C = f(S_{BET})$ are observed not in the entire range of NPs annealing temperatures. This dependence of the capacitance on the specific surface area of the compact sets indicates that the dielectric constant of the compacted nanopowder material depends not only on the surface area, but also on the water saturation of the material, and, consequently, on the level of atmospheric humidity. Determined from the dependencies in Fig. 5, the values of the dielectric constant of compact sets for nanopowders

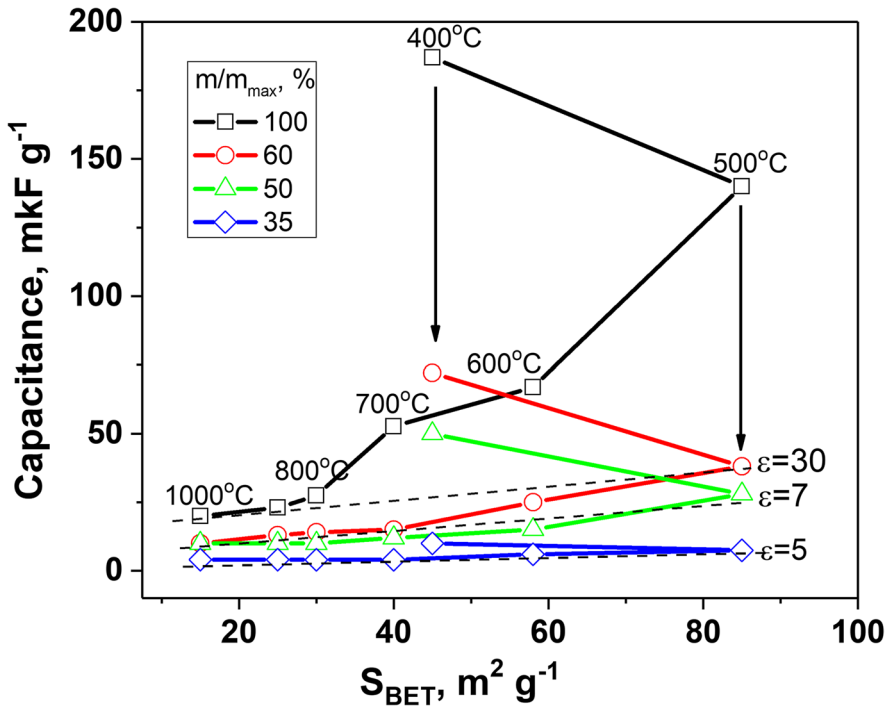

Fig. 5 Dependence of the specific capacitance of compact sets obtained from nanopowders synthesized at different temperatures on the specific surface area of the compact sets

synthesized at temperatures of 800–1000 °C were 30; for nanopowders synthesized at temperatures of 600–700 °C were 34; for a nanopowder synthesized at a temperature of 500 °C were 93; and for a nanopowder synthesized at a temperature 400 °C were 234. It should be noted that a reduction by 2 times in the water saturation of compact sets obtained from powder synthesized at 400 °C ($\Delta m / m_{max} = 50\%$) led to a decrease in the calculated dielectric constant to 34; and with a decrease in water saturation to 35%, the dielectric permeability decreased to 12. A similar picture is observed for compact sets obtained from powders synthesized at other annealing temperatures. That is, at low values of the moisture content of the samples (35%), the calculated value of the dielectric constant of the samples is 5–12, and with an increase in the value of moisture to the maximum level, which was used (6.5 wt%), increases to 234.

By analogy with the works (Zouaoui et al. 2016; Fripiat et al. 1966; Erjomina and Kostyukov 2008; Liu et al. 2013), such changes in the dielectric constant of materials from the degree of their hydration from one to hundreds is not unexpected and is associated with the influence of the orientational and interlayer polarization of water molecules on the dielectric constant of a hydrated heterogeneous system with an increase in the amount of adsorbed water.

For further analysis of the dielectric properties of compact sets, the EIS method was used.

Dependence of the impedance of compacted NPs on the temperature of their synthesis

The hodographs of the impedance of compacted NPs synthesized at different annealing temperatures are shown in Fig. 6. The arrow indicates the direction of increasing the frequency of the excitation signal. As can be seen, the hodographs of the impedance of compact sets obtained from nanopowders annealed at different temperatures have a similar shape. Data processing by DRT analysis showed a significant effect of low-frequency (electrode) polarization on relaxation processes. Removal of this influence using the RelaxIS 3 software allowed to receive correct hodographs of impedance with which further calculations were carried out. The hodograph consists of two regions with different geometries: a fragment of a circular arc in the high-frequency region and

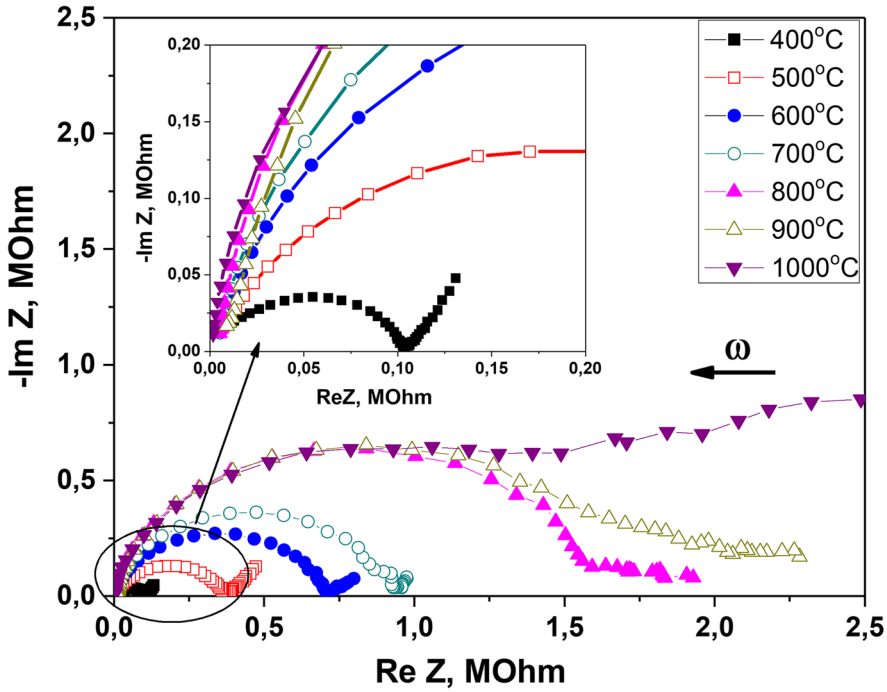

Fig. 6 Hodographs of impedance of compacted NPs with different annealing temperatures

a rectilinear low-frequency section in the low-frequency region.

The real part of the impedance (Z′) of compacted NPs synthesized at different temperatures as a function of frequency are shown in Fig. 7a. For all samples, a typical dependence of Z′ on frequency is fixed. It can be seen that in the low-frequency region the value of Z′ depends on the frequency and rapidly decreases depending on the temperature of NPs synthesis. At higher frequencies (about 100 kHz), the values of Z′ become constant and practically do not depend on the temperature of NPs synthesis. The imaginary part of the impedance Z″ of compacted NPs obtained at different temperatures as a function of frequency are shown in Fig. 7b. The intensity of the broad peak gradually decreases with decreasing NPs synthesis temperature, since the impedance value decreases with decreasing NPs synthesis temperature. This peak frequency, called the relaxation frequency, shifts toward higher frequencies as the NPs synthesis temperature decreases, which may mean that the hopping rate of localized charge carriers increases (Bharathi et al. 2011). For NPs synthesized at high temperatures (800 and 900 °C), an increase in Z″ is caused by a very large value of the active component of the sample resistance, approaching the measurement boundaries of the measuring device. For this reason, we did not analyze the impedance of a compacted NPs obtained at temperature of 1000 °C.

Influence of the synthesis temperature on the dielectric characteristics of compact sets

The study of the dielectric properties for any material is necessary to obtain valuable information about the polarization behavior, the mechanisms of conduction, and dielectric relaxation in the material. It is important to note that the dielectric constant is not constant. It can vary depending on the frequency, temperature, pressure, and molecular structure of the material.

The values of the real (ε′) and imaginary (ε″) parts of the electrical constant were calculated from the values of the real (Z′) and imaginary (Z″) parts of the impedance using formulas (Davidson and Cole 1951):

$$\varepsilon' = \frac{l}{\omega S \varepsilon_0} \frac{Z''}{Z'^2 + Z''^2} \quad (6)$$

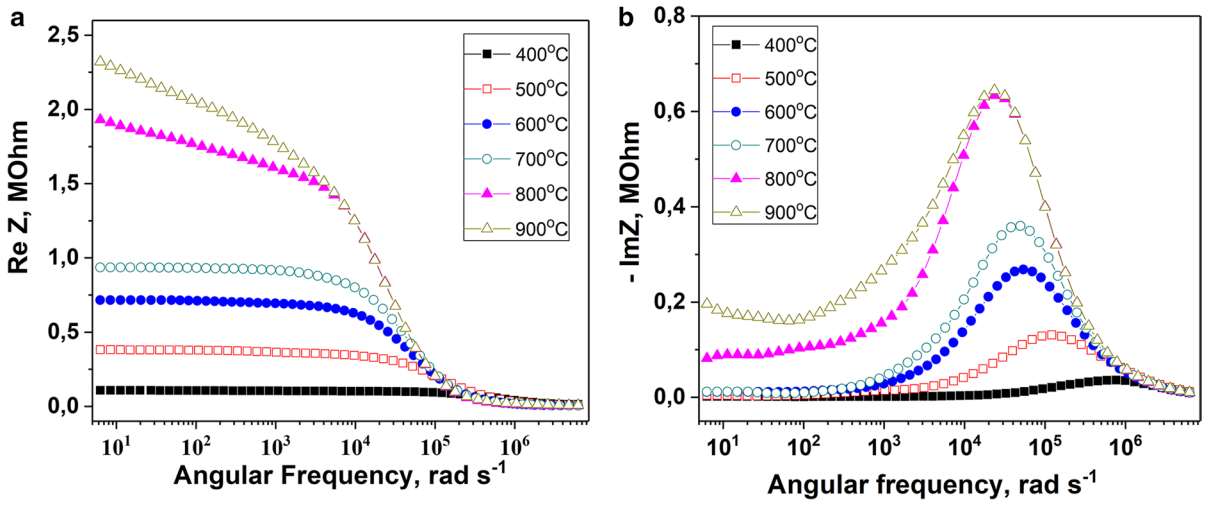

Fig. 7 Frequency dependences of the real (**a**) and imaginary (**b**) parts of the impedance of compacted nanoparticles synthesized at different temperatures

$$\varepsilon'' = \frac{l}{\omega S \varepsilon_0} \frac{Z'}{Z'^2 + Z''^2} \tag{7}$$

where l is the thickness of the sample; S is the cross-sectional area of the sample; ω is the angular frequency; and ε_0 is the electrical constant.

To approximate the experimental data, we used the Debye model with the distribution of relaxation times by Davidson and Cole (1951):

$$\varepsilon - \varepsilon_\infty = \frac{\varepsilon_s - \varepsilon_\infty}{(1 + i\frac{\omega}{\omega_0})^\beta} \tag{8}$$

where ε_s and ε_∞ are the values of the static and high-frequency dielectric constant, respectively, ω_0 is the relaxation angular frequency, and β is an empirical parameter, $0 < \beta < 1$.

After separating the real and imaginary parts, expression (8) has the form:

$$\varepsilon' - \varepsilon_\infty = (\varepsilon_0 - \varepsilon_\infty)(\cos\phi)^\beta \cos\beta\phi \tag{9}$$

$$\varepsilon'' = (\varepsilon_0 - \varepsilon_\infty)(\cos\phi)^\beta \sin\beta\phi \tag{10}$$

where $\mathrm{tg}\varphi = \omega / \omega_0$.

The frequency dependences of ε′ and ε″ of compact sets obtained from NPs with different annealing temperature are shown in Fig. 8. It can be seen from the figure that the dielectric constant is high in the low-frequency region for all samples; but as the frequency increases, the dielectric constant typically decreases due to the inability of relaxation processes to observe variations in the external alternating electric field.

It can be noted that the presence of water in the sample (a decrease in the temperature of NPs synthesis) significantly increases the values of ε′ and ε″ in the low frequency range. This phenomenon can be associated with several processes: increased electrical conductivity, ionic, and dipole relaxation. A rather low value of the relaxation frequency ($10–10^3$ Hz) gives grounds to assume that the orientational relaxation of water molecules makes an insignificant contribution to this process, since the characteristic time of orientational relaxation is $10^8–10^{10}$ Hz.

The values of the parameters of the Debye equation for compacted hydrated NPs that are calculated using Eq. 9 are given in Table 5. It is seen that the value of static dielectric constant increases with decreasing temperature of NPs synthesis.

Substitution of the static dielectric constant values into the formula of a plate capacitor allows one to calculate the value of the capacitance of a capacitor filled with compacted hydrated zirconia particles synthesized at different temperatures. When using the NPs synthesized at 400 °C, the capacitance is 191 μF g^{-1}, and when using the powder synthesized

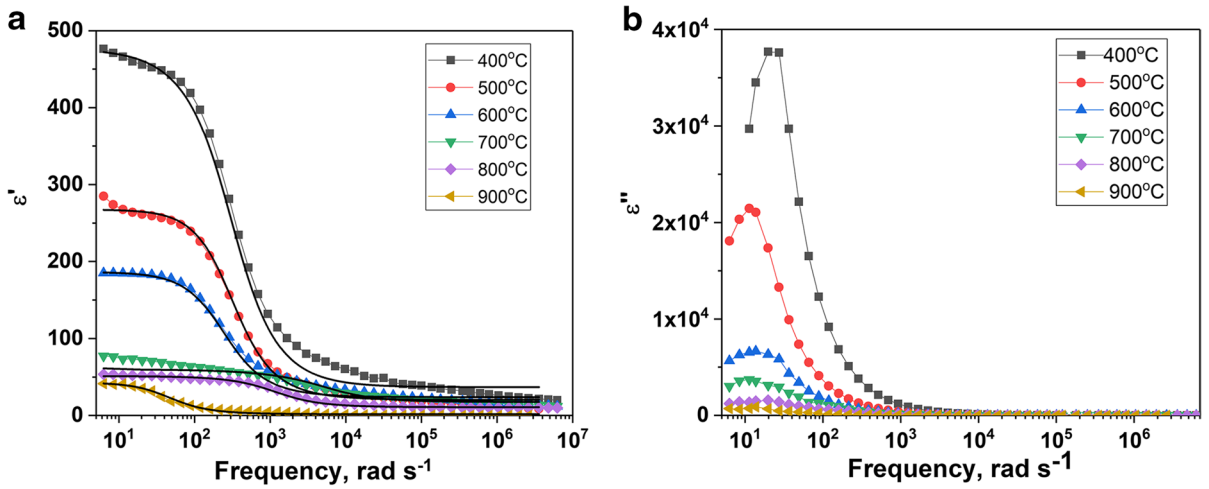

Fig. 8 Frequency dependences of the real (**a**) and imaginary (**b**) components of the dielectric constant for compacted NPs synthesized at different temperatures

at 700 °C, it is 30 μF g^{-1}, which is very close to the value of the capacitance determined from Fig. 5.

Since a heterogeneous system — NPs (ionic dielectric) and water molecules (polar dielectric) — demonstrates a significant increase in the capacitance with a decrease in the frequency of the electric field, which depends on the number of water molecules on the NPs surface (which is determined by the NPs annealing temperature), we can explain that this effect is due to the action of the interlayer polarization of water molecules, or the Maxwell–Wagner polarization, which leads to a significant increase in the dielectric constant of the heterogeneous hydrated nanomaterial.

In a dielectric material, as a rule, dielectric loss occurs due to the absorption of electrical energy used to rotate the dipole molecules. If the material contains regions with different dielectric properties, Maxwell–Wagner polarization arises at the interface between these regions. When an electric current passes through these interfaces, and when the dielectric parameters of these materials satisfy the condition $\sigma_1\varepsilon_2 \neq \sigma_2\varepsilon_1$, surface charges accumulate at the interfaces, which leads to the process of Debye relaxation with a characteristic frequency.

In our case, the model object can be represented as dielectric NPs covered with an adsorbed layer of water. That is, in the proposed model, two types of dielectric are interconnected — an ionic dielectric (zirconia) and a polar dielectric (water) — and these types of dielectrics are characterized by different times for establishing polarization (it is known that when setting atomic polarization, it is 10^{-10}–10^{-13} s, and the establishment time of the dipole and ionic polarization is 10^{-8}–10^{-2} s). In the samples studied in this work, when an electric field is applied, oppositely charged ions under the action of electrostatic forces begin to move in opposite directions, and spatial separation of charges occurs, which leads to the appearance of polarization. The contribution of this type of polarization to the overall polarization of the medium increases with an increase in the electrical contrast of its components, that is, it depends on the number of water layers on the surface of zirconia NPs.

Table 5 Calculated values of the Debye equation parameters for compacted zirconia NPs

Annealing temperature, °C	ε_s	ε_∞	ω_0	β
400	488	8.2	318	0.76
500	267	10	312	0.72
600	186	13	287	0.63
700	85	15.7	479	0.64
800	75	15.5	567	0.65
900	60	15.3	440	0.8

Conclusions

The effect of charge accumulation by compacted NPs of zirconia, the manifestation of which depends on the size of the particles (synthesis temperature of the NPs) and the degree of hydration of their surface, has been discovered. A decrease in the particle size from 32 to 9 nm (a decrease in the synthesis temperature from 1000 to 400 °C) leads to an increase in the potential difference at the electrodes of compacted NPs to 1.72 V, while the capacity increases by an order of magnitude (from $2 \bullet 10^{-5}$ to $1.87 \bullet 10^{-4}$ F g^{-1}) at the maximum degree of hydration.

Analysis of EIS data has shown that such an increase of capacitance with decreasing temperature of the nanoparticle synthesis is explained by a change in the sizes ε' and ε'' in the low frequency range. The change in dielectric constant is explained based on the two-layer Maxwell–Wagner model for space charge or interphase polarization. Such polarization is caused by the accumulation of free charge at the interfaces between the components of a heterogeneous medium, which has different values of electrical conductivity and dielectric constant.

Acknowledgements The authors are thankful the H2020-MSCA-RISE-2019 Program, project 871284 SSHARE and RO-JINR Program: Grant № 367/2021 item 27 for support of this work.

Declarations

Conflict of interest The authors declare that the research was conducted in the absence of any commercial or financial relationships that could be construed as a potential conflict of interest.

References

Andrievsky RA, Ragulya AV (2005) Nanostructured materials. Academy, Moscow

Bharathi KK, Marakandeyulu G, Ramana CV (2011) Impedance spectroscopic characterization of Sm and Ho doped Ni ferrites. J Electrochem Soc 158:71–78. https://doi.org/10.1149/1.3534800

Chevalier J, Gremillardw L (2009) The tetragonal–monoclinic transformation in zirconia: lessons learned and future trends. J Am Ceram Soc 92:1901–1920. https://doi.org/10.1111/j.1551-2916.2009.03278.x

Chysovitina TV, Toporov YuS, Tretnikova MG (1991) Properties of ceramics based on zirconia partly stabilized with yttrium concentrate. Refract and Indust Cer 32:277–279

Danilenko I, Gorban O, Shylo A, Akhkozov L, Lakusta M, Konstantinova T (2017) New multifunctional zirconia composite nanomaterials – from electronics to ceramics. IOP Conf. Series: Mater Sci and Eng 213:012016–012024. https://doi.org/10.1088/1757-899X/213/1/012016

Davidson DW, Cole RH (1951) Dielectric relaxation in glycerol, propylene glycol, and n-propanol. J Chem Phys 19:1484–1490. https://doi.org/10.1063/1.1748105

Doroshkevich AS, Danilenko IA, Konstantinova TE et al (2010) Structural evolution of zirconia nanopowders as a coagulation process. Crystallogr Rep 55:863–865. https://doi.org/10.1134/S1063774510050275

Erjomina NV, Kostyukov NS (2008) Water monolayer polarization on the surface of the insulator. Izvestia Samara Sci Center Russian Acad Sci 10:775–781

Fripiat JJ, Jelli A, Poncelet G, Andre J (1966) Thermodynamic properties of adsorbed water molecules and electrical conduction in montmorillonites and silicas. J Phys Chem 69:2185–2197. https://doi.org/10.1021/j100891a007

Groza JR, Dowding RJ (1996) Nanoparticle Material Densification Nanostruc Mater 7:749–768

Hsu HY, Chang KH, Salunkhe RR, Hsu CT et al (2013) Synthesis and characterization of mesoporous Ni–Co oxy–hydroxides for pseudocapacitor application. Elecrtochem Acta 94:104–112. https://doi.org/10.1016/j.pnsc.2015.11.012

Kelly JR, Denry I (2008) Stabilized zirconia as a structural ceramic: an overview. Dent Mater 24:289–298. https://doi.org/10.1016/j.dental.2007.05.005

Konstantinova TE, Ragulea AV, Doroshkevich AS et al (2006) The mechanisms of particle formation in Y–doped ZrO_2. Int J Nanotechnology 3:29–38

Konstantinova TE, Danilenko IA, Glazunova VA, Volkova GK, Gorban OA (2011) Mesoscopic phenomena in oxide nanoparticles systems: processes of growth. J Nanopart Res 13:4015–4023

Lewandowski A, Jakobczyk P, Galinski M, Biegun M (2013) Self-discharge of electrochemical double layer capacitors. Phys Chem Chem Phys 15:8692–8699. https://doi.org/10.1039/c3cp44612c

Lewis NS, Crabtree G, Nozik AJ et al (2005) Report on the basic energy sciences workshop on solar energy utilization. US Department of Energy, Office of Basic Energy Science, Washington DC. https://doi.org/10.2172/899136

Liu C, Zhang L, Peng J, Srinivasakannan C et al (2013) Temperature and moisture dependence of the dielectric properties of silica sand. J Microwave Power EE 47:199–209. https://doi.org/10.1080/08327823.2013.11689858

Lyubchyk A, Águas H, Fortunato E et al (2017) Experimental evidence for chemo-electronic conversion of water adsorption on the surface of nanosized yttria-stabilized zirconia. In: V.E. Borisenko, S.V. Gaponenko (eds) Phys, chem and appl of nanostruct: Rev and Short notes to Nanomeeting. Minsk, pp 257 – 262

Maier J (2005) Nanoionics: ion transport and electrochemical storadge in confined system. Nature Mater 4:805–815. https://doi.org/10.1038/nmat1513

Nguyen T, Montemor M (2019) Metal oxide and hydroxide-based aqueous supercapacitors: from charge storage mechanisms and functional electrode engineering

to need-tailored devices. Adv Sci 6:1801797–1801838. https://doi.org/10.1002/advs.201801797

Patterson AL (1939) The Scherrer Formula for X-Ray Particle Size Determination. Phys Rev 56:978–982

Pendashteh A, Rahmanifar MS, Mousavi MF (2014) Morphologically controlled preparation of CuO nanostructures under ultrasound irradiation and their evaluation as pseudocapacitor materials. Ultrason Sonochem 21:643 – 652. https://doi.org/10.1016/j.ultsonch.2013.08.009

Thakare V (2012) Progress in synthesis and applications of zirconia. Int J Eng Res Dev 5:25–28

Thompson DP, Dickins AM, Thorp JS (1992) The dielectric properties of zirconia. J Mater Sci 27:2267–2271. https://doi.org/10.1007/BF01117947

Yin L, Nakanishi Y, Alao AR, Song XF et al (2017) A review of engineered zirconia surfaces in biomedical applications. Proc CIRP 65:284–290. https://doi.org/10.1016/j.procir.2017.04.057

Zouaoui MJ, Nait-Ali B, Glandut N, Smith DS (2016) Effect of humidity on the dielectric constant and electrical impedance of mesoporous zirconia ceramics. J Eur Ceram Soc 36:163–169. https://doi.org/10.1016/j.jeurceramsoc.2015.09.008